

SemiEpi: Self-driving, Closed-loop Multi-Step Growth of Semiconductor Heterostructures Guided by Machine Learning

Chao Shen^{1,2}, Wenkang Zhan^{1,2}, Kaiyao Xin^{2,3}, Shujie Pan^{1,4}, Xiaotian Cheng⁵, Ruixiang Liu⁵, Zhe Feng⁵, Chaoyuan Jin⁵, Hui Cong^{2,6}, Chi Xu^{2,6}, Bo Xu^{1,2}, Tien Khee Ng⁷, Siming Chen^{1,2}, Chunlai Xue^{2,6}, Zhanguo Wang^{1,2}, and Chao Zhao^{1,2,*}

¹ Laboratory of Solid State Optoelectronics Information Technology, Institute of Semiconductors, Chinese Academy of Sciences, Beijing 100083, China

² College of Materials Science and Opto-Electronic Technology, University of Chinese Academy of Science, Beijing 101804, China

³ State Key Laboratory of Superlattices and Microstructures, Institute of Semiconductors, Chinese Academy of Sciences, Beijing 100083, China

⁴ HS Photonics Co., Ltd., Xiangjiang Science & Technology Innovation Base, Changsha, Hunan 413000, China

⁵ College of Information Science and Electronic Engineering, State Key Laboratory of Silicon and Advanced Semiconductor Materials, Zhejiang University, Hangzhou, China

⁶ Key Laboratory of Optoelectronic Materials and Devices, Institute of Semiconductors, Chinese Academy of Sciences, Beijing 100083, China

⁷ Photonics Laboratory, King Abdullah University of Science and Technology (KAUST),
Thuwal 23955-6900, Saudi Arabia

*Email: zhaochao@semi.ac.cn

Abstract

The semiconductor industry has prioritized automating repetitive tasks through closed-loop, self-driving experimentation, enabling the accelerated optimization of complex multi-step processes. The emergence of machine learning (ML) has ushered in self-driving processes with minimal human intervention. In this work, we introduce SemiEpi, a self-driving platform designed to execute molecular beam epitaxy (MBE) growth of semiconductor heterostructures through multi-step processes, in-situ monitoring, and on-the-fly feedback control. By integrating standard reactor, parameter initialization, and multiple ML models, SemiEpi identifies optimal initial conditions and proposes experiments for multi-step heterostructure growth, eliminating the need for extensive expertise in MBE processes. SemiEpi initializes material growth parameters tailored to specific material characteristics, and fine-tuned control over the growth process is then achieved through ML optimization. We optimize the growth for InAs quantum dots (QDs) heterostructures to showcase the power of SemiEpi, achieving a QD density of $5 \times 10^{10} \text{ cm}^{-2}$, a 1.6-fold increased photoluminescence (PL) intensity and reduced full width at half maximum (FWHM) of 29.13 meV. This work highlights the potential of closed-loop, ML-guided systems to address challenges in multi-step growth. Our method is critical to achieve repeatable materials growth using commercially scalable tools. Furthermore, our strategy facilitates developing a hardware-independent process and enhancing process repeatability and stability, even without exhaustive knowledge of growth parameters.

KEYWORDS: Molecular beam epitaxy, Quantum dots, Machine learning, Reflective high-energy electron diffraction, Self-driving

Introduction

In recent years, automation has shown significant potential to transform research by streamlining traditionally repetitive tasks and executing self-driving experiments with minimal human involvement.¹ Automation tools have been successfully applied to small-molecule synthesis, photocatalytic reactions, and organic laser discovery.^{2,3} However, semiconductor growth poses unique challenges due to its inherent complexity, comprising multiple interdependent variables such as growth temperature, flux, and growth rate. The traditional way to identify the optimal growth condition involves trial and error and relies heavily on the expertise and resources of molecular beam epitaxy (MBE) growers, making it both time-consuming and resource-intensive.^{4,5} Consequently, only a small subset of the parameter space can be systematically explored during optimization. Additionally, dynamic fluctuations in equipment conditions, including sample holders, reactors and their environments, as well as variability in substrates from different batches, can render predetermined parameters and fixed programs ineffective.^{6,7}

Semiconductor heterostructures serve as a fundamental building block of modern devices. The multi-step growth of these layers requires optimizing numerous parameters and tailored epitaxial growth for individual layers, further increasing the process complexity. The growth of quantum dot (QD) heterostructures presents additional challenges, including the precise control over QD size, shape, and density to achieve device performance requirements.⁸⁻¹⁰ The conventional growth of QD heterostructure involves sequential substrate deoxidation, buffer layer growth, and Stranski-Krastanow (SK) growth of QDs. The complex multi-step growth process in a high-dimensional experimental space presents significant challenges.^{11,12}

Machine learning (ML) has been employed to uncover relationships between dynamic growth and resulting material properties to optimize growth parameters.^{13,14} However, this approach relies

on previously collected growth data and might not generalize effectively to subsequent growth. It cannot mitigate system fluctuations, particularly in temperature—a parameter that is both directly measurable and critically influential. These fluctuations result in variability in QD density, rendering preset temperature profiles insufficient for achieving optimal growth conditions.^{15,16} Reconstruction transitions, typically observed in situ via reflective high-energy electron (RHEED), vary depending on the substrate material's inherent physical properties. These transition-related characteristic temperatures can be used to mark and provide more suitable material growth temperatures.^{17,18} Integrating in-situ feedback control and closed-loop decision-making assisted by RHEED is essential.^{19,20} In this context, we reported substrate deoxidation and on-demand QD growth using ML and feedback control.^{21,22} However, initial conditions still necessitate human intervention, and the process for multi-step growth of heterostructures remains undeveloped. A widely applicable self-driving, multi-step growth process incorporating parameter initialization could substantially expand the accessibility of high-quality heterostructures.

Researchers have developed automated systems to optimize material growth characteristics, which leverage prior experimental data to refine parameters for subsequent growth processes.²³⁻²⁵ For instance, Ryota Shimizu et al. optimized material preparation parameters but requires transferring the material to a separate chamber for adjustments, which precludes real-time optimization.²⁶ Similarly, AlphaFlow performs multi-step experiments in a closed loop but necessitates completing microdroplet mixing before sample analysis, limiting its ability to adjust growth parameters during synthesis.¹ Additionally, proper initialization is essential to minimize deviations during growth and reduce the need for real-time adjustments required to achieve optimal outcomes. While recent reports have proposed architectures for parameter initialization and the

prediction of material growth outcomes using in situ data, these methodologies have yet to be implemented or integrated into dynamic control frameworks.^{27,28}

A robust platform is essential to address these challenges by integrating closed-loop, multi-step processes and enabling real-time optimization. It should prioritize the proper initialization of growth conditions, develop predictive models for material outcomes, and ensure dynamic optimization of growth parameters. In our work, we introduce SemiEpi, a self-driving platform designed to perform multi-step MBE growth under optimal conditions. It features a self-driving method for adjusting growth temperatures, coupled with an in-situ monitoring and feedback control system using ML to grow InAs QDs as a demonstrative structure. The platform correlates in situ RHEED videos with surface reconstruction and QD growth. It generates a parameter initialization curve, selects an initial growth temperature, and fine-tunes the substrate temperature during growth using ML models without human intervention. This capability enables the customization of growth conditions for individual substrates, marking a significant milestone in establishing a precise growth control scheme and closed-loop experimentation strategies. This way, we can intelligently optimize multi-step growth within a complex parameter space, previously only possible through time-consuming, labor-intensive experimentation and human intervention.

Results

Design of SemiEpi

SemiEpi was developed to address the challenge of optimizing complex multi-step growth conditions. After heterostructure design, three critical modules of SemiEpi operate sequentially: substrate deoxidation, parameter initialization, and material growth (see Fig. 1a). It facilitates continuous in-situ monitoring, self-optimization, and on-the-fly feedback control to grow specific

structures. The substrate deoxidation module removes amorphous oxides from the substrate surface to ensure a fresh growth front. The substrate temperature is gradually increased until the deoxidation feature is observed through in-situ RHEED, and the deoxidation temperature is subsequently recorded (see Fig. 1b). Following parameter initialization, the 100-nm GaAs is re-grown at a theoretical temperature of 600 °C based on the parameter initialization results. The substrate is subsequently cooled to a theoretical temperature of 490 °C for sequential growth of buried InAs QDs, followed by a 10-nm GaAs layer. The temperature is then raised to a theoretical temperature of 600 °C to grow an additional 100-nm GaAs. Finally, the substrate is cooled to the temperature used for buried InAs QDs growth, and the surface InAs QDs are grown starting from this temperature.

The parameter initialization module monitors the reconstruction state of the material surface by RHEED and simultaneously obtains the corresponding thermocouple temperature. As the substrate is heated or cooled, changes in surface energy and stress cause the surface atoms to rearrange, allowing different reconstruction states to be observed.²⁹ Additionally, a transition temperature is associated with the interconversion of these states. For instance, as the substrate temperature increases, the surface energy decreases, weakening the bond between the As cap and the GaAs surface, resulting in the desorption of the As cap from the GaAs surface at a theoretical temperature of 350 °C.³⁰ As the temperature further increases, the reconstruction transitions from $c(4\times 4)$ to (2×4) at a theoretical temperature of 510 °C, followed by a transition from (2×4) to $(n\times 6)$ at a theoretical temperature of 620 °C (see Fig. 1c).³¹ By recording the deoxidation temperature and several transition thermocouple temperatures, SemiEpi establishes the relationship between the thermocouple and theoretical temperatures (see Fig. 1d). The temperature can then be adjusted to

better align with the theoretical temperature for material growth, thus reducing the need for significant change in subsequent processes.

The material growth module performs heterostructure growth, it records real-time data, including temperature and shutter status, and feeds this pre-processed data into the ML model for further processing. Hardware acceleration, controlled by software, will be employed to enhance data processing efficiency (see Fig. 1e). It also monitors the material' status during growth and employs ML models to identify conditions that require optimization. This enables dynamic feedback control of the growth parameters. The ML model can efficiently analyze a large amount of in-situ monitoring data. The module operates in a closed-loop manner; real-time growth information obtained during the material growth process is fed back into the ML model, resulting in new insights that guide parameter optimization until the desired conditions are met.

Combining ML with on-the-fly feedback control, SemiEpi automates execution and analysis. This approach allows for dynamic optimization of these parameters within a single experiment, minimizing the need for multiple experimental runs and resulting in more efficient and effective material growth. SemiEpi is a self-driving setup that offers significant advantages over conventional methods by customizing growth conditions for each substrate, ensuring compatibility across different reactors without requiring code modifications. It eliminates the need for extensive semiconductor or MBE process expertise to achieve best results, making it a valuable platform for use in any epitaxy laboratory regardless of the grower's level of knowledge and experience.

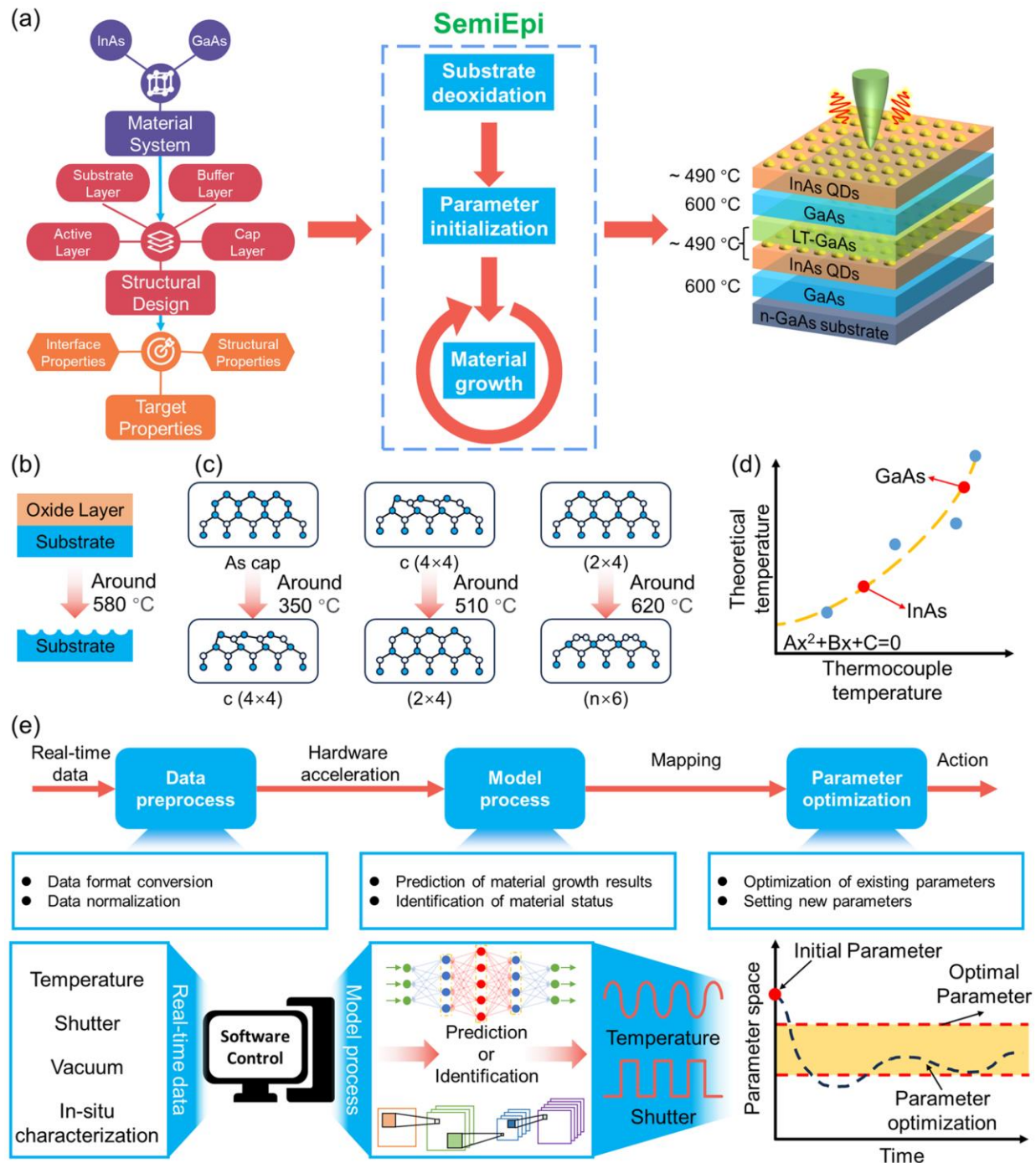


Fig. 1: Overview of SemiEpi. (a) SemiEpi’s framework. Before operating SemiEpi, the reactor is configured according to the design of the heterostructure. The operation involves three modules that work sequentially to grow samples with specified structures. Schematic of (b) substrate deoxidation, (c) surface reconstruction, (d) parameter initialization, and (e) material growth.

SemiEpi software

Existing industrial software operates as closed, procedural systems where data on material growth and characterization is not integrated. This lack of integration hinders effective data fusion between these two software systems, complicating real-time adjustments to growth parameters. Additionally, most industrial software prioritizes automating predefined steps rather than intelligently evaluating or adjusting the growth state based on real-time data.

In our work, SemiEpi was developed using LabVIEW. It uses NI-VISA to control parameters for MBE, such as temperature and the shutter. It also utilizes NI VISION to acquire RHEED video from the fluorescent screen. The acquired data is processed using Python libraries and transferred to the ML model, formatted in ONNX and optimized with TensorRT for faster inference (see Supplementary Information for the platform environment and program interface and the functional interface switch in the program, S1 and S2). Before initiating the platform, the grower measures the beam flux of cells and sets the cells' temperatures according to structure design. The Modbus protocol can swiftly adapt to temperature controllers with different addresses, enabling commands to be read and written to different controllers.

SemiEpi hardware

SemiEpi combines a standard reactor, a camera, temperature controllers, shutter controllers, and an in-situ RHEED system to enable monitoring and optimization. It was designed and deployed on a Windows 10 system with an AMD R9 7950X CPU, 64GB of RAM, an NVIDIA 3090 graphics card, and a 2TB solid-state drive. The system is linked to a temperature controller and a shutter controller via USB 2.0 for data exchange. The Modbus protocol enables the connection of

multiple temperature controllers in series and precise control of the In and Ga cells using addresses. Additionally, USB 3.0 allows the connection of a camera in a dark room outside the fluorescent screen. Furthermore, the model training and data preprocessing processes used by SemiEpi are also conducted on the system (see Supplementary Information for the deployment environment and hardware wiring scheme, S3).

Data acquisition and feature analysis

The electron beam from the RHEED gun interacts with the continuously rotating sample, producing a diffracted pattern on the fluorescent screen. A reminder is triggered to ensure adequate time to manually open the RHEED fluorescent screen shutter before capturing and preprocessing real-time RHEED images, which are then sent to the ML model for analysis (see Fig. 2a). The preprocessing methods used in this study align with previously reported methods.²¹ Each frame of the RHEED data is processed as a single channel of luminance information. These processed data are then stacked along an additional dimension to form a three-dimensional array, which serves as the input sample for the model. Thus, RHEED data are continuously recorded and analyzed in real-time, enabling precise determination of the critical transition temperature. While manual adjustments to the RHEED power supply and the fluorescent screen shutter were necessary in this study, these processes could be improved for computer control by integrating an RHEED system with the optional “microprocessor controlled beam current regulation” feature and upgrading the fluorescent screen shutter to an automatic control system.^{32,33}

Gathering as many temperature points as possible is essential to obtain the parameter initialization curve. SemiEpi focuses on several vital temperatures, such as the deoxidation temperature, the transition temperature of As cap/c(4×4), c(4×4)/(2×4), and (2×4)/(n×6) (see Fig.

2a). We reported RHEED characteristics of GaAs deoxidation, corresponding to the theoretical temperature of 580 °C.^{34,35} After deoxidation, the substrate temperature is reduced and subsequently increased to observe the transition from the As cap to the (n×6) stage.^{36,37} By observing the brightness and spacing of RHEED streaks from different angles, the ×4 reconstruction line can be identified from two angles, corresponding to c(4×4) (see Fig. 2b-c). As the temperature increases, thermal vibrations of surface atoms intensify, leading to atomic reconstructions. Consequently, a gradual transition from c(4×4) to (2×4) can be observed around the theoretical temperature of 510 °C (see Fig. 2d-e).³¹ When the temperature exceeds a theoretical temperature of 620 °C, the (2×4) becomes increasingly blurred, and the (n×6) gradually appears due to the lattice expansion of the GaAs crystal.^{29,38} In this study, ×2 and ×6 reconstruction line can be observed from two angles, corresponding to the (2×6) structure (see Fig. 2f-g).

We used a dataset of 38 samples to develop our models. Of these, 8 samples were GaAs substrates observed at different temperatures. Since the GaAs surface undergoes a gradual transformation, we collected data from each sample multiple times, with each video lasting at least 20 minutes. The remaining 30 samples were InAs QDs grown under various conditions. The growth process for each of these samples was repeated multiple times, with each video recording lasting at least 90 seconds. The dataset used for model training consists of various RHEED images, including clear and blurred examples. During data preprocessing, we applied image augmentation techniques, including adjustments to brightness, saturation, and contrast, along with the noise addition to simulate various levels of blurriness and other effects that could result from manual adjustments to the RHEED power supply.³⁹⁻⁴¹ Additionally, we utilized random image cropping to mimic the effects of varying beam positions on the sample, which influences the range of patterns displayed. We then converted images into single-channel intensity images for model

input.⁴² This approach enabled the model to effectively process more degraded images during validation, enhancing its generalizability and resulting in approximately 370,000 NumPy arrays.

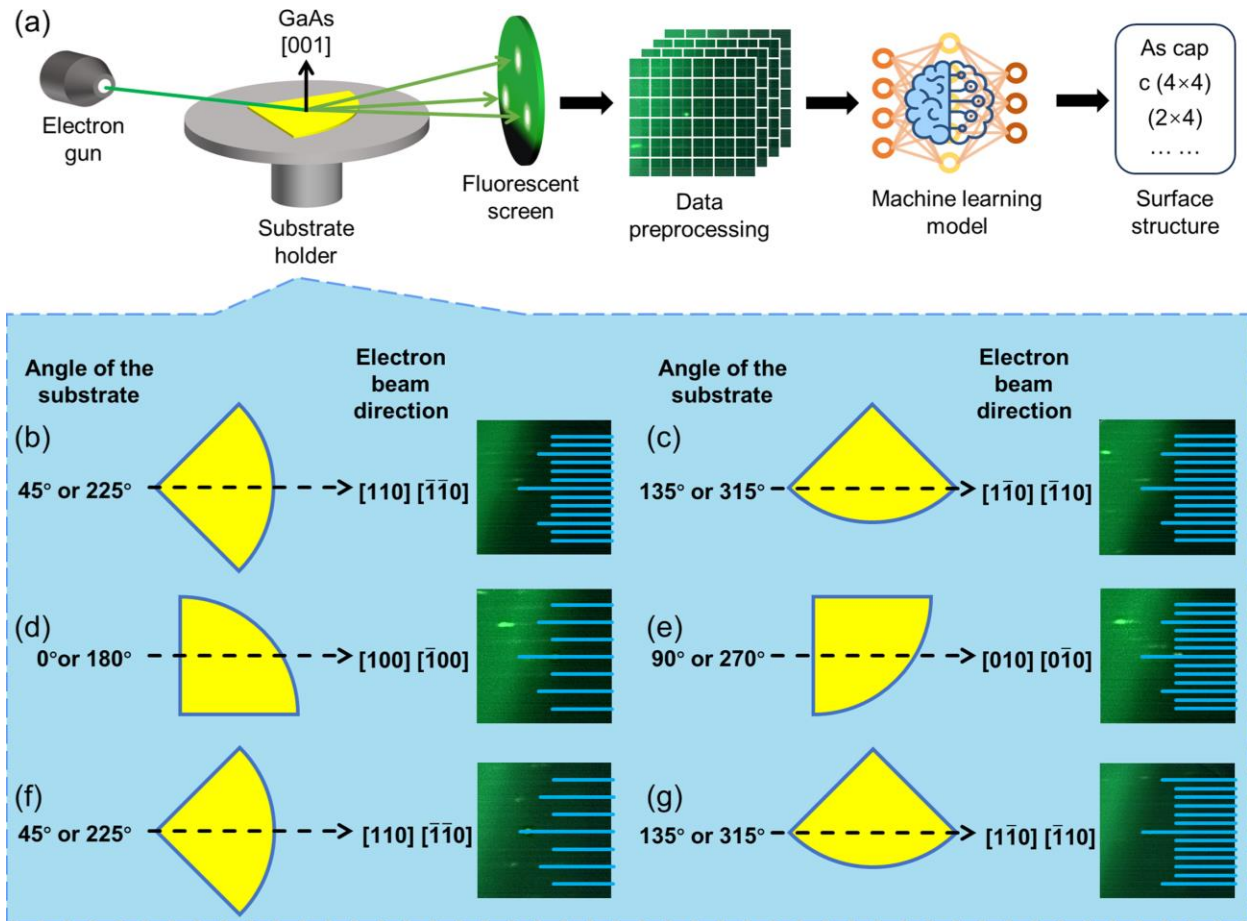


Fig. 2: RHEED data acquisition and feature analysis of the reconstruction. (a) Workflow for RHEED data acquisition and processing. (b-g) Typical RHEED images obtained at various substrate angles. The blue lines on the images represent reconstruction streaks. Longer solid blue lines indicate integer order streaks, while shorter solid lines denote fractional order streaks.

Model construction and evaluation

The conventional convolutional neural network (CNN) approach processes all color channels in an image simultaneously, integrating information from each channel to extract features. This is effective for images with rich color information.^{43,44} However, it is less practical for datasets

comprising multiple stacks of single-channel luminance information, such as RHEED data acquired from different angles of a continuously rotating substrate. To address this issue, a model must emphasize channel information, strengthen inter-channel correlations, and enhance data processing efficiency.^{45,46} Therefore, we introduce the global attention residual network and cross-layer adaptive fusion (GARN-CAF) model, specifically developed to prioritize channel information. This study constructs three GARN-CAF models to analyze RHEED data of different material growth steps, namely, “Reconstruction model”, “Temperature model”, and “Shutter model” (see Fig. 3a). These models are designed for a multi-class classification task, with the “Reconstruction model” identifying reconstruction and deoxidation states, the “Temperature model” predicting the optimal InAs growth temperature, and the “Shutter model” evaluating the completion conditions for InAs QD growth.

The GARN-CAF model consists of GARN and CAF blocks. GARN block first maps input features to a reduced number of channels through convolutional layers (see Fig. 3b).^{47,48} Several generalized attention residual blocks follow this, each comprising two convolutional layers and a channel attention mechanism which adjusts the contribution of each channel by globally pooling the feature map and calculating importance weights.^{49,50} Finally, a downsampling layer and an additional convolutional layer further process the feature map, reducing its spatial resolution to generate the final output. The CAF block leverages a transformer-based architecture to process image data (see Fig. 3c).^{51,52} The image is divided into small blocks, and their features are embedded through linear transformations. The transformer’s attention mechanism captures global dependencies between image blocks and processes cross-layer associations. Traditional CNN can lead to the loss of vital angle-dependent diffraction details. In contrast, the CAF mechanism excels at processing RHEED images by dynamically adjusting feature channel weights, where essential

diffraction information shifts at various angles due to substrate rotation and wobbling. This mechanism allows the CAF to effectively model contextual relationships between different image blocks, enhancing the recognition of complex patterns.⁵³ The model's feed-forward network further processes these features, which are finally classified using a multilayer perceptron. This adjustment enables the GARN-CAF model to identify and extract critical features more accurately, a crucial capability for detecting subtle feature changes in images captured at varying angles.

The number of stacks in the model is crucial for delivering richer input, especially when analyzing RHEED data, which experiences periodic changes. Not all frames of RHEED images provide informative data across all angles. If the number of image stacks is too small, the training samples may include significant irrelevant or non-informative data. This can lead to inconsistent training outcomes, unstable validation performance, and even overfitting. Therefore, we optimized the model input sizes and determined that the best training performance was achieved using 24 images per batch, each with a resolution of 128×128 pixels (see Fig. 3d-e). The accuracy is calculated as the ratio of correctly predicted labels to the total number of predictions.^{54,55} In our work, we selected the cross-entropy loss function, a well-established choice for classification tasks. This function guides the model in adjusting its weights and biases by minimizing the loss, thereby enhancing the precision of predictions.^{55,56} To expedite the training process, we employed the stochastic gradient descent optimizer, which effectively updates the model parameters during each iteration.^{54,57} The resulting validation accuracies for the "Reconstruction model", "Temperature model", and "Shutter model" reached 99.1%, 99.6%, and 99.9%, respectively.

We analyzed alignment features of the "Reconstruction model". Using t-Distributed Stochastic Neighbor Embedding (t-SNE) analysis, we observed a clear separation between different color points, indicating the model effectively identifies both deoxidation and various reconstruction

states (see Fig. 3f).⁵⁸⁻⁶⁰ We also extracted two frames of typical RHEED maps from a sample, both showing prominent $\times 2$ (see Fig. 3g-h). By plotting the convolutional features map, we observed that the convolution primarily focuses on streak-like features in RHEED images, which correspond to different reconstruction streaks, demonstrating high interpretability (see Fig. 3i-j). When analyzing the attention heat map of the model with these two typical RHEED frames as inputs, it is evident that non-streak features appear dark, indicating that the model did not focus on these regions (see Fig. 3k-l). Conversely, the brighter regions highlight streak-shaped features. Feature maps were also combined from multiple images to identify focal regions across the model. These plots highlight streak features on the left side (see Fig. 3m). In contrast, the right side, consisting of non-streak features, is mainly flat. This indicates the model effectively focuses on regions with distinct features. Additionally, we used Gradient-weighted Class Activation Mapping (Grad-CAM) to analyze the contribution of each region to the classification results (see Fig. 3n).⁶¹⁻⁶³ The Grad-CAM results highlight multiple streak features, which align well with the streak feature locations in the input image, demonstrating that the model has high sensitivity in data processing.

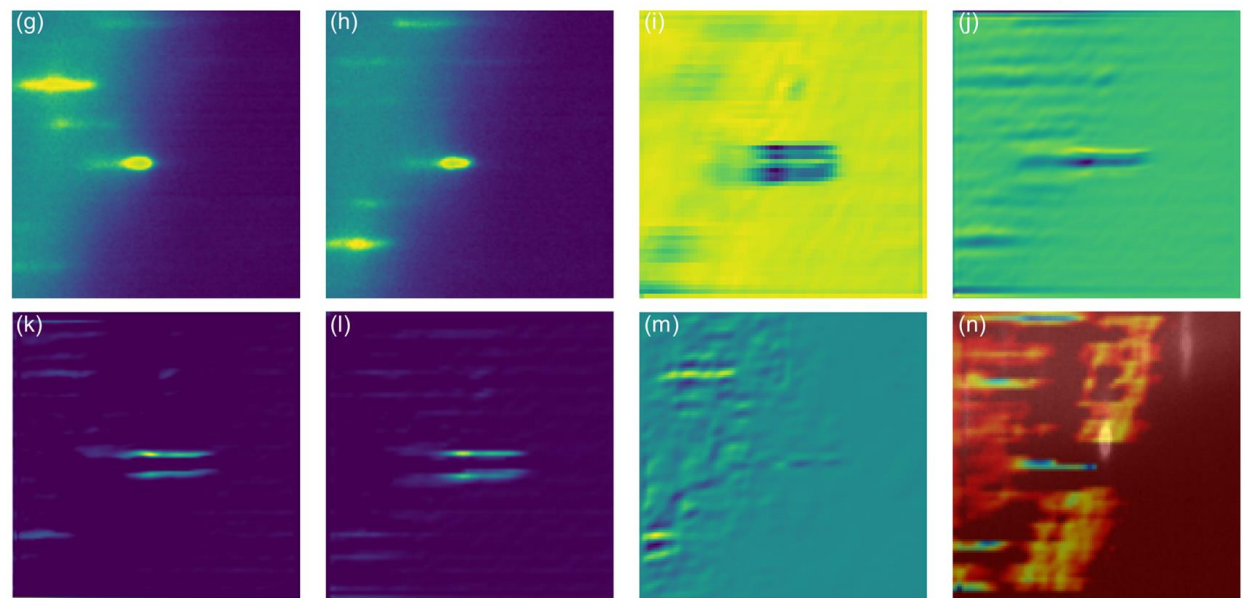
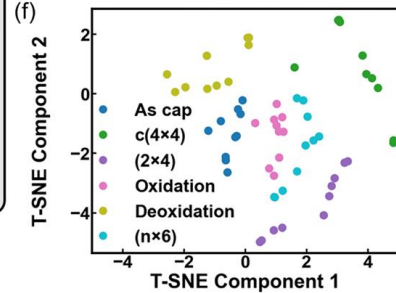
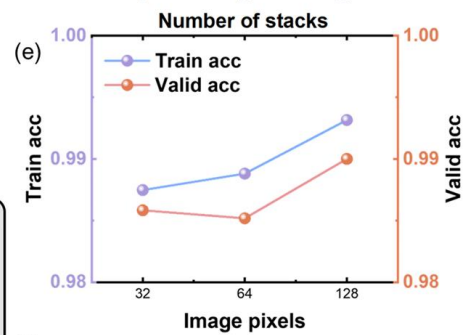
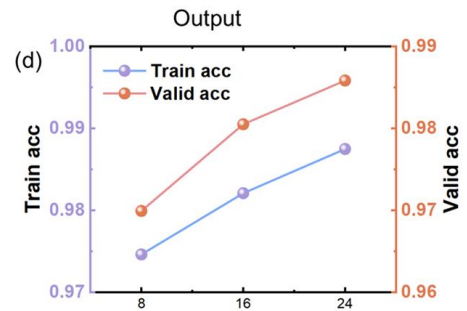
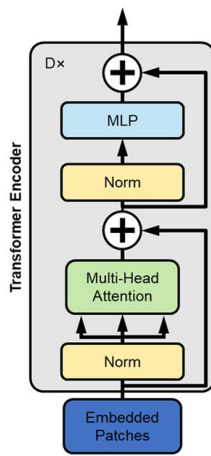
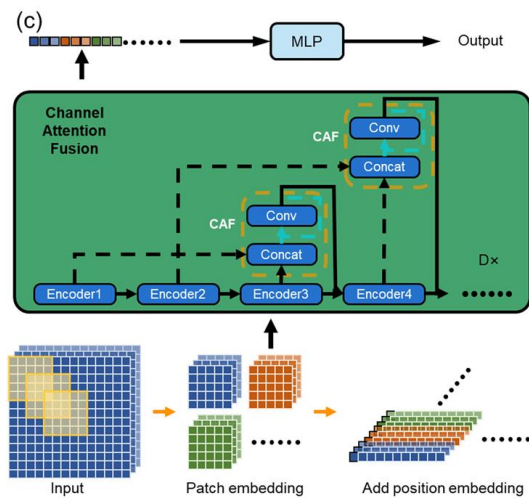
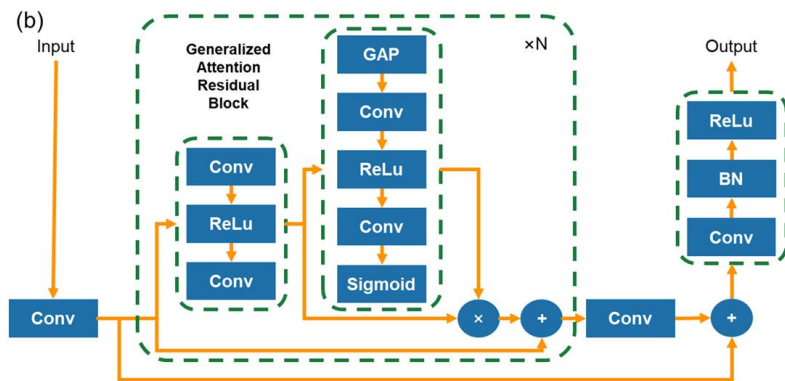
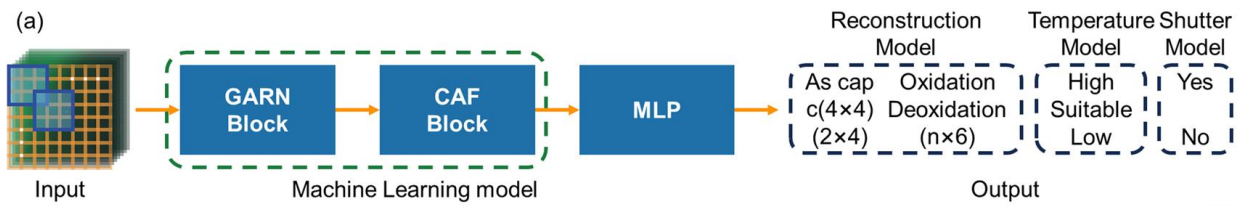


Fig. 3: Model construction and evaluation. (a) A simplified architectural diagram of the model. The structure of the (b) GARN and (c) CFA blocks. Conv: convolutional layer. ReLu: rectified linear unit activation layer. GAP: global average pooling layer. Sigmoid: sigmoid activation layer. BN: batch normalization layer. Encoder: transformer encoder. MLP: multilayer perceptron. The variation of model validation accuracy and validation loss under different (d) heads and depths and (e) image stacks. Model feature processing: (f) t-SNE visualization of high-dimensional features. (g-h) Typical RHEED images. (i-j) Convolutional layer feature maps, (k-l) Attention heat maps, (m) Combined feature map, (n) Gradient-weighted class activation mapping results.

The “Reconstruction model” and the “Shutter model” are discriminative models that evaluate the material’s state, identifies and optimizes the InAs QD growth conditions in real time. In contrast, the “Temperature model” is a predictive model that forecasts the performance of samples upon growth completion. This model facilitates real-time predictions of QD density during growth, enabling timely parameter adjustments and ensuring high-quality material growth.

Experiment validation

Parameter initialization

In our study, thermocouples are used to measure temperatures; however, temperature readings from multiple reconstruction transition points exhibit a non-linear relationship with the corresponding theoretical temperatures. A curve fitting approach is necessary to achieve a more reliable correlation.^{64,65} We compared different curve-fitting methods and found that the quadratic curve-fitting results were better than those obtained with linear or higher-order polynomial fits (see Supplementary Information for the comparison results from different function fits, S5).

The parameter initialization curve extracts the thermocouple temperatures corresponding to the growth conditions to achieve the desired QD density, which can be achieved at a growth theoretical temperature of 490 °C with a low growth rate. While it is possible to optimize the growth temperature for GaAs during the process, variations around the theoretical temperature of 600 °C have minimal impact on the quality of the material (see Supplementary Information for the surface morphology and crystal quality of GaAs grown at different temperatures, S6). Therefore, with the parameter initialization curve, the thermocouple temperatures corresponding to the theoretical temperature of 490 °C and 600 °C were established for the growth of InAs QDs and GaAs.

The main objective of SemiEpi is to generate parameter initialization curves and optimize growth parameters for InAs QDs with desired density. Real-time data recorded by SemiEpi around different transition points was analyzed (see Fig. 4). During the automatic deoxidation process, SemiEpi heated up in increments of 5 °C, from the thermocouple temperature of 390 °C to 415 °C through five increments (see Fig. 4a). The RHEED screen showed no distinctive features until the thermocouple temperature of 415 °C, when distinct bright spot features appeared (see Fig. 4e-f). Analysis of the “Reconstruction model” output during deoxidation revealed that, from the 0th to around the 16,000th sequence, the oxidation probability remained close to 1, indicating that the model did not identify the deoxidation state. After the 16,000th sequence, the deoxidation probability rapidly increased to nearly 1, confirming the model’s accurate identification of the deoxidation state (see Fig. 4b).

After growing a layer of GaAs on the deoxidized sample and cooling, the substrate was gradually heated at a rate of 15 °C per minute (see Fig. 4c). Real-time RHEED data collected during this process was analyzed using the “Reconstruction model” to monitor reconstruction states (see Fig. 4d). Initially, the model identified only “As cap” labels, with RHEED patterns showing diffuse

features from the beginning to around the 2,000th sequence (see Fig. 4g-h). By around the 3,000th sequence, at a thermocouple temperatures at 135 °C, a marked shift occurred as the probability of “As cap” labels dropped sharply and “c(4×4)” labels became dominant. The RHEED patterns began exhibiting periodic features consistent with the emergence of a ×4 reconstruction (see Fig. 4i-j). At around the 11,000th sequence, as the substrate heating reached 353°C, the probability of “(2×4)” labels increased significantly. This shift indicated a structural change on the surface, supported by RHEED observations of features combining ×2 and ×4 (see Fig. 4k-l). Finally, by the 14,000th sequence, the model output showed an increased probability for the “(n×6)” label. At this stage, the thermocouple temperature reached 455 °C, and the RHEED patterns displayed a distinct ×6 periodicity alongside residual ×2 features (see Fig. 4m-n). The results demonstrate the model’s high sensitivity in distinguishing between different structural states.

Finally, SemiEpi used a quadratic curve to fit the collected thermocouple temperature data to theoretical temperature data. This set the initial thermocouple temperatures for InAs growth at 330 °C and for GaAs growth at 436 °C (see Fig. 4o).

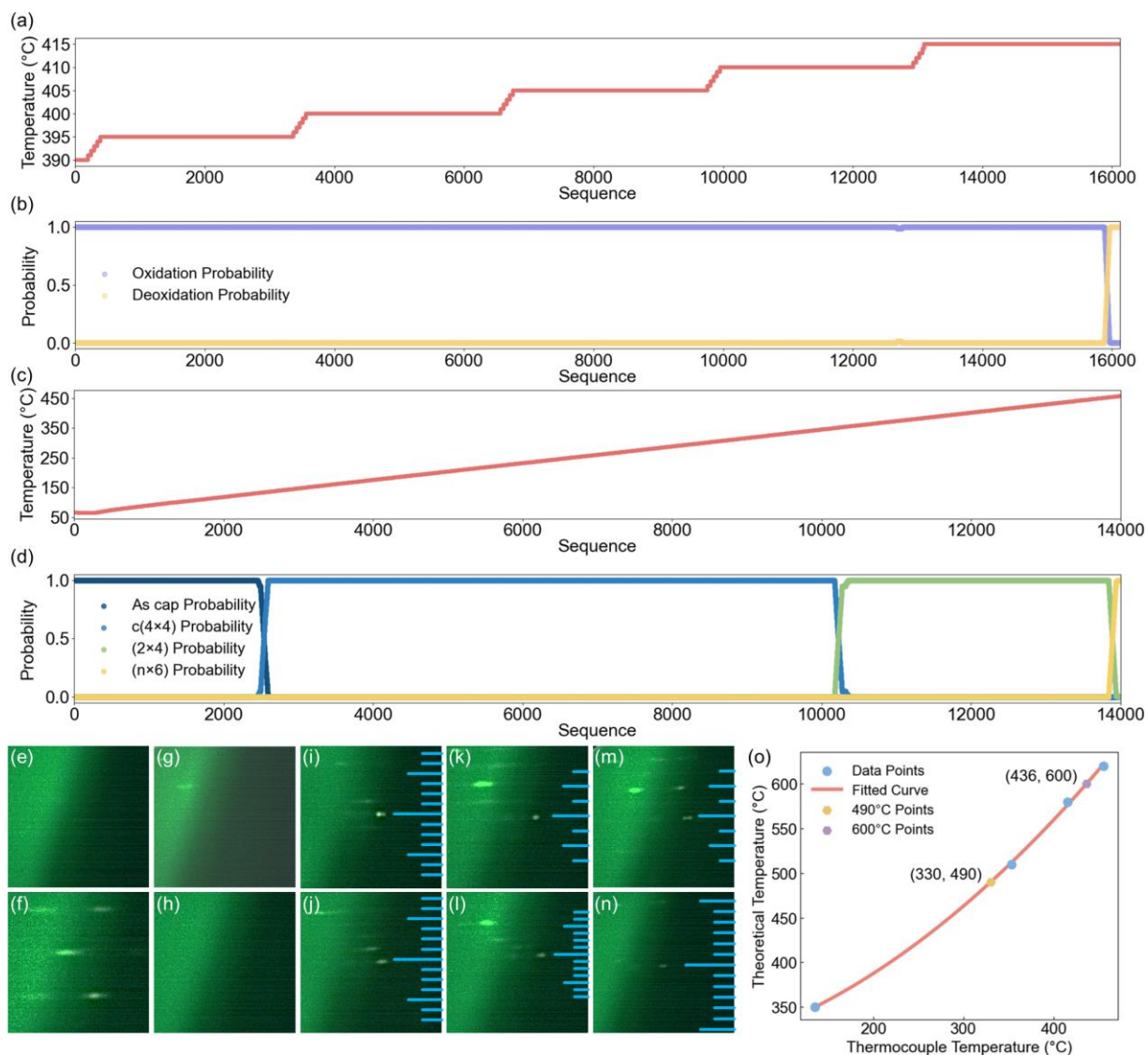


Fig. 4: The parameter initialization. Acquisition of the deoxidation temperature: (a) The temperature variation curve of the substrate. (b) The output results of the “Reconstruction model” and the statistical results of the moving average method. Acquisition of the reconstruction temperature: (c) The temperature variation curve of the substrate. (d) The output results of the “Reconstruction model” model and the statistical results of the moving average method. The RHEED image captured at around (e) 13,000th and (f) 16,000th sequence of (a); (g-h) 2,000th, (i-j) 3,000th, (k-l) 11,000th and (m-n) 14,000th sequence of (c). Each pair of RHEED images was

captured from two angles. (o) Parameter initialization results. Source data are provided as a Source Data file.

QD growth

The density of InAs QDs is highly sensitive to temperatures; SemiEpi uses RHEED to analyze the material surface and optimize the temperature in real-time to ensure that the samples achieve the desired density range of $4\text{-}6 \times 10^{10} \text{ cm}^{-2}$ (see Fig. 5) (see Supplementary Video for the experiment).^{66,67} During the growth of buried InAs QDs, the thermocouple temperature analysis revealed a 2 °C decrease, consistent with the trend of QD density change relative to thermocouple temperature (see Fig. 5a and Supplementary Information for the variation in QD density with thermocouple temperature, S7). This indicates that the initial temperature alone does not ensure achieving the desired density range. Statistical analysis of RHEED data using the “Temperature model” reveals that, in the early stages, the model predominantly outputs the “High” label (see Fig. 5b). As growth progresses, the probability of the model outputting the “Suitable” label increases around the 200th sequence. Subsequently, the model mainly outputs “Suitable” labels, with this label becoming more likely towards the end of the growth. The probability of the “Low” label remains consistently low, indicating the initial growth temperature was too high and required adjustment to achieve the desired density.

The “Shutter model” analysis indicates that from the 0th to approximately the 1200th sequence, the model primarily outputs “No”, suggesting the InAs QD growth has not yet achieved the desired density (see Fig. 5c). However, at the 1300th sequence, the probability of outputting “Yes” gradually increases, indicating the desired QD density is achieved. Analysis of RHEED data reveals that from the 100th and 700th sequences, RHEED patterns exhibit evident streak characteristics

with no QDs formed (see Fig. 5d-e). In contrast, RHEED patterns from the 1300th sequence reveal well-formed, rounded, and neatly aligned spots, indicating successful QD formation (see Fig. 5f).

Additionally, the sample prepared using SemiEpi exhibited a photoluminescence (PL) intensity of 3605 and a full width at half maximum (FWHM) of 29.13 meV. This performance significantly surpassed that of the reference sample prepared using conventional methods, which exhibited a PL intensity of 2270 and an FWHM of 34.70 meV. Additionally, it outperformed the reference sample prepared using parameter initialization, which exhibited a PL intensity of 2531 and an FWHM of 30.79 meV (see Fig. 5g and Supplementary Information for the reference sample prepared using conventional methods and the reference sample prepared using parameter initialization, S8 and S9). Additionally, time-resolved photoluminescence (TRPL) measurements were also conducted to assess the quality of the QDs. The obtained effective lifetimes of 2.06 ns demonstrate the high quality of the QDs, providing strong evidence for the reliability of SemiEpi (see Supplementary Information for the time-resolved photoluminescence results, S10). SemiEpi also grew surface InAs QDs to observe their morphology. The initial growth temperature for these QDs was set to the thermocouple temperature of 328 °C, which was the temperature for buried InAs QDs (see Fig. 5h). During growth, the thermocouple temperature remained stable at 328 °C. This highlights that adjusting the temperature during the growth of buried InAs QDs allowed achieving the desired QD density without the need for additional temperature adjustments.

The probabilistic statistical analysis of the “Temperature model” output during the process shows that initially, the model predominantly outputs “Suitable” labels, with only a few “High” labels (see Fig. 5i). This indicates that the initial growth temperature is appropriate. The analysis of the “Shutter model” output reveals a significant increase in the probability of the “Yes” label at the 1300th sequence, indicating that the QDs have achieved the desired QD density (see Fig. 5j).

In the RHEED patterns obtained at the 100th, 700th, and 1300th sequences, we observe a transition from streak to spot features as the growth progresses (see Fig. 5k-m). The spot pattern at the 1300th sequence appears well-ordered and rounded. AFM characterization of the surface InAs QDs indicates a high QD density of approximately $5 \times 10^{10} \text{ cm}^{-2}$, with a relatively uniform distribution (see Fig. 5n). In addition, the reference sample prepared using parameter initialization achieved a density of $5.4 \times 10^{10} \text{ cm}^{-2}$. However, the reference sample prepared using conventional methods only achieved a QD density of $3.7 \times 10^{10} \text{ cm}^{-2}$, falling below the range designated as “Suitable”. This highlights the effectiveness of parameter initialization in improving growth outcomes.

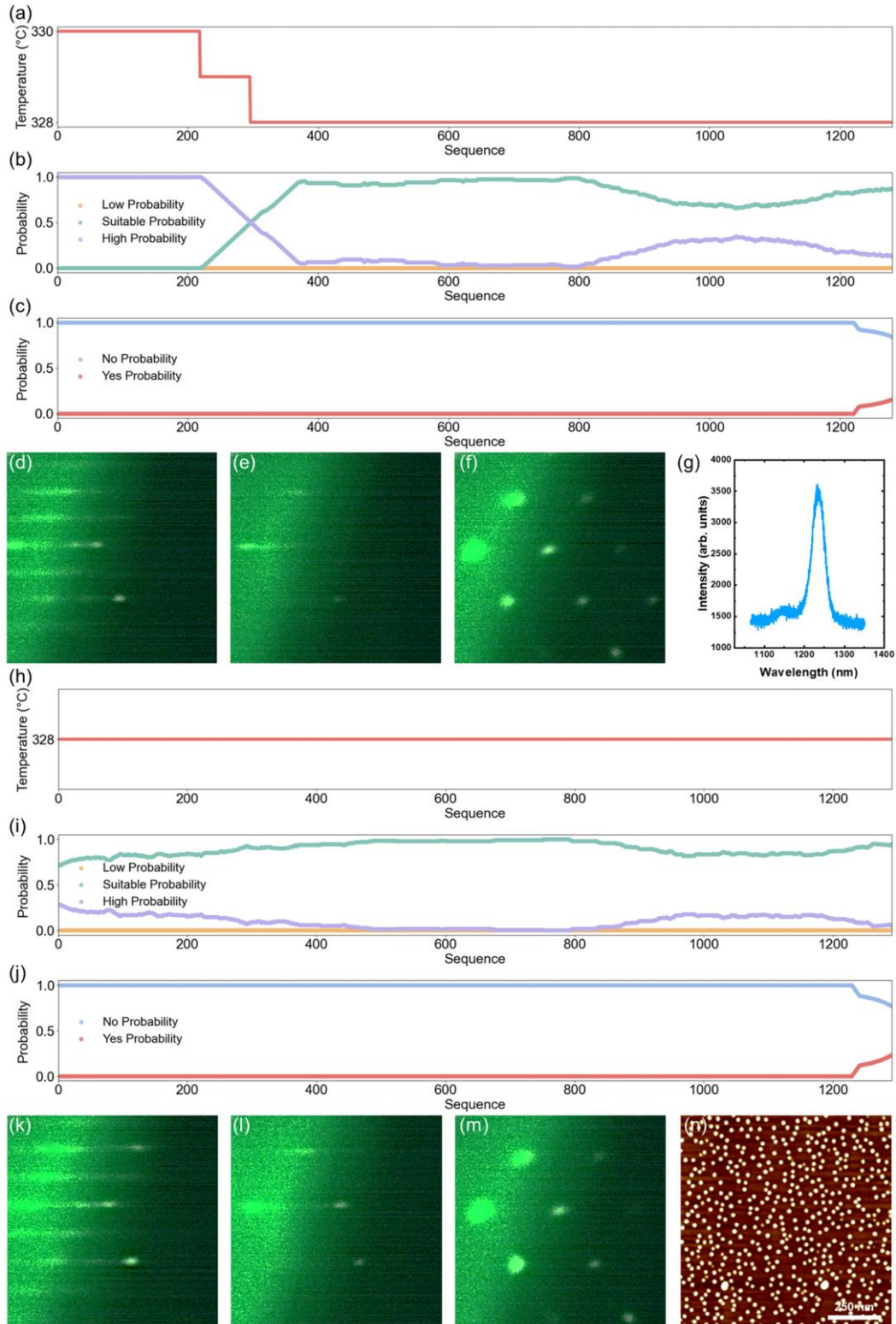


Fig. 5: The growth of the InAs QDs. Buried InAs QDs: (a) The temperature variation curve of the substrate. (b) The output results of the “Temperature model” and the statistical results of the

moving average method. (c) The output results of the “Shutter model” and the statistical results of the moving average method. The RHEED image captured (d) at around the 100th sequence of (a), (e) at around the 700th sequence of (a) and (f) at around the 1300th sequence of (a). (g) Photoluminescence spectrum of QDs. Surface InAs QDs: (h) The temperature variation curve of the substrate. (i) The output results of the “Temperature model” and the statistical results of the moving average method. (j) The output of the “Shutter model” and the statistical results of the moving average method. The RHEED image captured (k) at around the 100th sequence of (h), (l) at around the 700th sequence of (h), and (m) at around the 1300th sequence of (h). (n) The sample’s 1 $\mu\text{m} \times 1 \mu\text{m}$ AFM image. Source data are provided as a Source Data file.

Discussion

In this work, we successfully developed a self-driving approach for heterostructures growth using SemiEpi. We build upon existing methods to optimize growth steps by integrating fundamental physical knowledge of semiconductor substrates. Given a desired structure, the algorithm utilizes existing growth data in the database to establish initial conditions. These conditions are then proposed for experimental validation across a range of temperatures. They are iteratively monitored and analyzed using ML algorithms to predict the outcome. We aligned the thermocouple temperature with the theoretical temperature by parameter initialization. SemiEpi thus selects an optimal starting growth temperature and dynamically adjusts it during the InAs QDs growth process, efficiently mapping the relationships between material states and their outcomes, improving material quality and ensuring more consistent and reliable results.

The QDs’ performance using SemiEpi aligns with the expected characteristics of QD lasers.⁶⁸⁻
⁷⁰ However, our experiments are facing some challenges, including a failure rate associated with

temperature change rates and the similarity of data characteristics. The similarity in RHEED patterns between the As cap layer and the oxidation state complicates the identification process and impacts the dataset construction. This emphasizes the need for more accurate labeling and clearer differentiation between these states.

In summary, SemiEpi integrates ML models, prior semiconductor knowledge, and feedback control during experiments, offering a promising pathway toward developing a universal method to address hardware disparities between systems, often leading to unpredictable results. This platform overcomes the limitations of traditional methods, which rely on fixed programs and are highly sensitive to reactor geometry, status, and sample inconsistencies. Identifying growth stages and minimizing result variations across different reactors to achieve parameter initialization ensures reproducible growth conditions. This capability is especially crucial for managing complex multi-step growth processes and can significantly improve the success rate of material growth. We utilized RHEED for analysis, but the system can quickly adapt to other techniques, such as absorption spectroscopy and mass spectrometry. By enabling dynamic adjustments, SemiEpi effectively explores and optimizes the high-dimensional parameter space of in-situ data and material growth results, ensuring that growth conditions remain stable and reproducible, regardless of external fluctuations. Furthermore, this method can scale to large-scale material growth, reducing the parameter optimization cycle and improving material outcomes. Moving forward, a smart MBE system integrating portability, multimodality, and reinforcement learning could be expected to revolutionize material growth.

Methods

Material growth

The InAs QD samples were grown on GaAs substrates using a Riber 32P MBE reactor. The system is equipped with an arsenic (As) valved cracker, as well as indium (In) and gallium (Ga) effusion cells. During the growth process, the As₂ source was used, and the cracker temperature was maintained at over 900 °C. Beam Equivalent Pressure (BEP) measurements were used to assess the fluxes and calibrate the ratios of group III and V elements.⁷¹ Substrate temperatures were monitored using C-type thermocouples, and the growth rates were calibrated by observing RHEED oscillations from additional layers grown on the GaAs substrate. The BEP values for the cells were as follows: 6.8×10^{-9} Torr for In, 1.5×10^{-7} Torr and 9×10^{-8} Torr for Ga, and 2.5×10^{-6} Torr, 1.5×10^{-6} Torr, and 1.0×10^{-6} Torr for As used in GaAs, and InAs, respectively. Before the growth process, the n-GaAs substrates were outgassed in a buffer chamber at 350°C. The growth was managed by SemiEpi, which included steps for substrate deoxidation, surface reconstruction, parameter initialization, and material growth. The growth rates were 0.6 μm/h and 0.36 μm/h for GaAs, while the InAs growth rate was approximately 0.016 ML/s.

Material characterization

RHEED was set up in the MBE growth chamber with a power supply at 12 kV and 1.49 A to generate an electron beam (RHEED 12 from STAIB Instruments). The electron beam interacts with the surface of the epitaxial layer, producing diffraction patterns that are then projected onto a fluorescent screen. These patterns are captured in real-time via a camera mounted outside the chamber in a dark room. Throughout the growth process, the substrate was rotated at one revolution every 3 seconds. The camera had an exposure time of 100 ms and a sampling rate of 8 frames per second, meaning that every 24 frames represented one full revolution of the substrate. After the growth was completed, the samples were characterized using a custom-built PL system (iHR 550 spectrometers from HORIBA). This system consists of an optical beam splitter, reflector,

attenuator, and a 532 nm continuous wave excitation laser. An InGaAs detector within the spectrometer collected the light emitted by the samples. The surface morphology of the InAs QDs was also characterized using AFM (Dimension Icon from Burker). Time-resolved PL (TRPL) measurements were conducted at 130 K using a short-pulse laser (Chameleon Ultra from Coherent). The excitation power density was set at 0.76 W/cm. The emitted PL was analyzed with a spectrometer (FHR 1000 from Horiba) and detected using an infrared single-photon detector (ID230 Infrared Single-Photon Detector from Picoquant).

Data Availability

Source data are provided with this paper.

Code Availability

Source codes are provided within this paper. The ML model and LabVIEW program used can be found via Code Ocean at <https://codeocean.com/capsule/6854238/tree>.

References

- 1 Volk, A. A. *et al.* AlphaFlow: autonomous discovery and optimization of multi-step chemistry using a self-driven fluidic lab guided by reinforcement learning. *Nat. Commun.* **14**, 1403, doi:10.1038/s41467-023-37139-y (2023).
- 2 Slattery, A. *et al.* Automated self-optimization, intensification, and scale-up of photocatalysis in flow. *Science* **383**, eadj1817, doi:doi:10.1126/science.adj1817 (2024).
- 3 Strieth-Kalthoff, F. *et al.* Delocalized, asynchronous, closed-loop discovery of organic laser emitters. *Science* **384**, eadk9227, doi:doi:10.1126/science.adk9227 (2024).

- 4 Kwoen, J. & Arakawa, Y. Multiclass classification of reflection high-energy electron diffraction patterns using deep learning. *Journal of Crystal Growth* **593**, 126780, doi:10.1016/j.jcrysgro.2022.126780 (2022).
- 5 Scheel, H. J. Historical aspects of crystal growth technology. *Journal of Crystal Growth* **211**, 1-12, doi:[https://doi.org/10.1016/S0022-0248\(99\)00780-0](https://doi.org/10.1016/S0022-0248(99)00780-0) (2000).
- 6 Joyce, P. B. *et al.* Optimizing the growth of 1.3 μm InAs/GaAs quantum dots. *Physical Review B* **64**, 235317, doi:10.1103/PhysRevB.64.235317 (2001).
- 7 Liu, H. Y. *et al.* Optimizing the growth of 1.3 μm InAs/InGaAs dots-in-a-well structure. *Journal of Applied Physics* **93**, 2931-2936, doi:10.1063/1.1542914 (2003).
- 8 Walker, A. W., Thériault, O., Wheeldon, J. F. & Hinzer, K. The Effects of Absorption and Recombination on Quantum Dot Multijunction Solar Cell Efficiency. *IEEE Journal of Photovoltaics* **3**, 1118-1124, doi:10.1109/JPHOTOV.2013.2257920 (2013).
- 9 Gan, Z. X. *et al.* Quantum confinement effects across two-dimensional planes in MoS₂ quantum dots. *Applied Physics Letters* **106**, 233113, doi:10.1063/1.4922551 (2015).
- 10 Liu, J. *et al.* Size effects on structural and optical properties of tin oxide quantum dots with enhanced quantum confinement. *Journal of Materials Research and Technology* **9**, 8020-8028, doi:<https://doi.org/10.1016/j.jmrt.2020.05.041> (2020).
- 11 Wang, T. *et al.* The effect of growth temperature of GaAs nucleation layer on InAs/GaAs quantum dots monolithically grown on Ge substrates. *Applied Physics Letters* **100**, 052113, doi:10.1063/1.3682314 (2012).
- 12 Wu, G., Wang, Y., Gong, Q., Li, L. & Wu, X. An Intelligent Temperature Control Algorithm of Molecular Beam Epitaxy System Based on the Back-Propagation Neural Network. *IEEE Access* **10**, 9848-9855, doi:10.1109/ACCESS.2022.3143811 (2022).

- 13 Choudhary, K. *et al.* Recent advances and applications of deep learning methods in materials science. *npj Computational Materials* **8**, 59, doi:10.1038/s41524-022-00734-6 (2022).
- 14 Mahmood, A., Irfan, A. & Wang, J.-L. Machine Learning for Organic Photovoltaic Polymers: A Minireview. *Chinese Journal of Polymer Science* **40**, 870-876, doi:10.1007/s10118-022-2782-5 (2022).
- 15 Junno, B., Jeppesen, S., Miller, M. S. & Samuelson, L. A comparison of RHEED reconstruction phases on (100) InAs, GaAs and InP. *Journal of Crystal Growth* **164**, 66-70, doi:[https://doi.org/10.1016/0022-0248\(96\)00009-7](https://doi.org/10.1016/0022-0248(96)00009-7) (1996).
- 16 Heitz, R., Mukhametzhanov, I., Madhukar, A., Hoffmann, A. & Bimberg, D. Temperature dependent optical properties of self-organized InAs/GaAs quantum dots. *Journal of Electronic Materials* **28**, 520-527, doi:10.1007/s11664-999-0105-z (1999).
- 17 Duke, C. B. Semiconductor Surface Reconstruction: The Structural Chemistry of Two-Dimensional Surface Compounds. *Chemical Reviews* **96**, 1237-1260, doi:10.1021/cr950212s (1996).
- 18 Bell, G. R., Belk, J. G., McConville, C. F. & Jones, T. S. Species intermixing and phase transitions on the reconstructed (001) surfaces of GaAs and InAs. *Physical Review B* **59**, 2947-2955, doi:10.1103/PhysRevB.59.2947 (1999).
- 19 Currie, K. R., LeClair, S. R. & Patterson, O. D. Self-Directed, Self-Improving Control of a Molecular Beam Epitaxy Process. *IFAC Proceedings Volumes* **25**, 83-87, doi:10.1016/s1474-6670(17)49469-9 (1992).
- 20 Currie, K. R. & LeClair, S. R. Self-improving process control for molecular beam epitaxy. *The International Journal of Advanced Manufacturing Technology* **8**, 244-251, doi:10.1007/bf01748634 (1993).

- 21 Shen, C. *et al.* Universal Deoxidation of Semiconductor Substrates Assisted by Machine Learning and Real-Time Feedback Control. *ACS Applied Materials & Interfaces* **16**, 18213-18221, doi:10.1021/acsami.4c01765 (2024).
- 22 Shen, C. *et al.* Machine-learning-assisted and real-time-feedback-controlled growth of InAs/GaAs quantum dots. *Nature Communications* **15**, 2724, doi:10.1038/s41467-024-47087-w (2024).
- 23 Nikolaev, P. *et al.* Autonomy in materials research: a case study in carbon nanotube growth. *npj Computational Materials* **2**, 16031, doi:10.1038/npjcompumats.2016.31 (2016).
- 24 MacLeod, B. P. *et al.* Self-driving laboratory for accelerated discovery of thin-film materials. *Science Advances* **6**, eaaz8867, doi:10.1126/sciadv.aaz8867.
- 25 Gongora, A. E. *et al.* A Bayesian experimental autonomous researcher for mechanical design. *Science Advances* **6**, eaaz1708, doi:10.1126/sciadv.aaz1708.
- 26 Shimizu, R., Kobayashi, S., Watanabe, Y., Ando, Y. & Hitosugi, T. Autonomous materials synthesis by machine learning and robotics. *APL Materials* **8**, 111110, doi:10.1063/5.0020370 (2020).
- 27 Harris, S. B. *et al.* Autonomous Synthesis of Thin Film Materials with Pulsed Laser Deposition Enabled by In Situ Spectroscopy and Automation. *Small Methods* **8**, 2301763, doi:<https://doi.org/10.1002/smt.202301763> (2024).
- 28 Fébba, D. M. *et al.* Autonomous sputter synthesis of thin film nitrides with composition controlled by Bayesian optimization of optical plasma emission. *APL Materials* **11**, 071119, doi:10.1063/5.0159406 (2023).
- 29 Ohtake, A. Surface reconstructions on GaAs(001). *Surface Science Reports* **63**, 295-327, doi:<https://doi.org/10.1016/j.surfrep.2008.03.001> (2008).

- 30 Karpov, I. *et al.* Arsenic cap layer desorption and the formation of GaAs(001)c(4×4) surfaces. *Journal of Vacuum Science & Technology B: Microelectronics and Nanometer Structures Processing, Measurement, and Phenomena* **13**, 2041-2048, doi:10.1116/1.588130 (1995).
- 31 Ohtake, A., Ozeki, M., Yasuda, T. & Hanada, T. Atomic structure of the GaAs(001)-(2×4) surface under As flux. *Physical Review B* **65**, 165315, doi:10.1103/PhysRevB.65.165315 (2002).
- 32 Conrad, R. & Mertens, P. A microprocessor-based beam sweep control unit. *Nuclear Instruments and Methods in Physics Research* **189**, 275-280, doi:[https://doi.org/10.1016/0029-554X\(81\)90154-3](https://doi.org/10.1016/0029-554X(81)90154-3) (1981).
- 33 Glawischnig, H. & Noack, K. in *Ion Implantation: Equipment and Techniques*. (eds Heiner Ryssel & Hans Glawischnig) 161-166 (Springer Berlin Heidelberg).
- 34 Cho, A. Y. Growth of III–V semiconductors by molecular beam epitaxy and their properties. *Thin Solid Films* **100**, 291-317, doi:[https://doi.org/10.1016/0040-6090\(83\)90154-2](https://doi.org/10.1016/0040-6090(83)90154-2) (1983).
- 35 Rei Vilar, M. *et al.* Characterization of wet-etched GaAs (100) surfaces. *Surface and Interface Analysis* **37**, 673-682, doi:<https://doi.org/10.1002/sia.2062> (2005).
- 36 Bernstein, R. W., Borg, A., Husby, H., Fimland, B. O. & Grepstad, J. K. Capping and decapping of MBE grown GaAs(001), Al_{0.5}Ga_{0.5}As(001), and AlAs(001) investigated with ASP, PES, LEED, and RHEED. *Applied Surface Science* **56-58**, 74-80, doi:[https://doi.org/10.1016/0169-4332\(92\)90218-M](https://doi.org/10.1016/0169-4332(92)90218-M) (1992).
- 37 Resch, U. *et al.* Thermal desorption of amorphous arsenic caps from GaAs(100) monitored by reflection anisotropy spectroscopy. *Applied Surface Science* **63**, 106-110, doi:[https://doi.org/10.1016/0169-4332\(93\)90072-J](https://doi.org/10.1016/0169-4332(93)90072-J) (1993).
- 38 Ohtake, A. Structure and composition of Ga-rich (6×6) reconstructions on GaAs(001). *Physical Review B* **75**, 153302, doi:10.1103/PhysRevB.75.153302 (2007).

- 39 Qi, Y. *et al.* A Comprehensive Overview of Image Enhancement Techniques. *Archives of Computational Methods in Engineering* **29**, 583-607, doi:10.1007/s11831-021-09587-6 (2022).
- 40 Khaireh-Walieh, A., Arnoult, A., Plissard, S. & Wiecha, P. R. Monitoring MBE Substrate Deoxidation via RHEED Image-Sequence Analysis by Deep Learning. *Crystal Growth & Design* **23**, 892-898, doi:10.1021/acs.cgd.2c01132 (2023).
- 41 Liang, H. *et al.* Application of machine learning to reflection high-energy electron diffraction images for automated structural phase mapping. *Physical Review Materials* **6**, 063805, doi:10.1103/PhysRevMaterials.6.063805 (2022).
- 42 Kim, H. J. *et al.* Machine-learning-assisted analysis of transition metal dichalcogenide thin-film growth. *Nano Convergence* **10**, 10, doi:10.1186/s40580-023-00359-5 (2023).
- 43 Jiang, J., Feng, X. a., Liu, F., Xu, Y. & Huang, H. Multi-Spectral RGB-NIR Image Classification Using Double-Channel CNN. *IEEE Access* **7**, 20607-20613, doi:10.1109/access.2019.2896128 (2019).
- 44 Xu, W., Gao, F., Zhang, J., Tao, X. & Alkhateeb, A. Deep Learning Based Channel Covariance Matrix Estimation With User Location and Scene Images. *IEEE Transactions on Communications* **69**, 8145-8158, doi:10.1109/tcomm.2021.3107947 (2021).
- 45 Codella, N. C. F. *et al.* Deep learning ensembles for melanoma recognition in dermoscopy images. *IBM Journal of Research and Development* **61**, 5:1-5:15, doi:10.1147/jrd.2017.2708299 (2017).
- 46 Reith, F., Koran, M. E., Davidzon, G. & Zaharchuk, G. Application of Deep Learning to Predict Standardized Uptake Value Ratio and Amyloid Status on ¹⁸F-Florbetapir PET Using ADNI Data. *American Journal of Neuroradiology* **41**, 980-986, doi:10.3174/ajnr.A6573 %J American Journal of Neuroradiology (2020).

- 47 Deng, S. & Dong, Q. GA-NET: Global Attention Network for Point Cloud Semantic Segmentation. *IEEE Signal Processing Letters* **28**, 1300-1304, doi:10.1109/LSP.2021.3082851 (2021).
- 48 Wang, M., Li, C. & Ke, F. Recurrent multi-level residual and global attention network for single image deraining. *Neural Computing and Applications* **35**, 3697-3708, doi:10.1007/s00521-021-06814-w (2023).
- 49 Feng, H. & Zhao, Y. mmWave RIS-Assisted SIMO Channel Estimation Based on Global Attention Residual Network. *IEEE Wireless Communications Letters* **12**, 1179-1183, doi:10.1109/LWC.2023.3265648 (2023).
- 50 Ou, Y., Chen, Z. & Wu, F. Multimodal Local-Global Attention Network for Affective Video Content Analysis. *IEEE Transactions on Circuits and Systems for Video Technology* **31**, 1901-1914, doi:10.1109/TCSVT.2020.3014889 (2021).
- 51 Li, G. *et al.* MCAFNet: multiscale cross-layer attention fusion network for honeycomb lung lesion segmentation. *Medical & Biological Engineering & Computing* **62**, 1121-1137, doi:10.1007/s11517-023-02995-9 (2024).
- 52 Cheng, S., Chan, R. & Du, A. CACFTNet: A Hybrid Cov-Attention and Cross-Layer Fusion Transformer Network for Hyperspectral Image Classification. *IEEE Transactions on Geoscience and Remote Sensing* **62**, 1-17, doi:10.1109/TGRS.2024.3374081 (2024).
- 53 Hong, D. *et al.* SpectralFormer: Rethinking Hyperspectral Image Classification With Transformers. *IEEE Transactions on Geoscience and Remote Sensing* **60**, 1-15, doi:10.1109/TGRS.2021.3130716 (2022).

- 54 Hassan, E., Shams, M. Y., Hikal, N. A. & Elmougy, S. The effect of choosing optimizer algorithms to improve computer vision tasks: a comparative study. *Multimedia Tools and Applications* **82**, 16591-16633 (2023).
- 55 Zhang, Z. & Sabuncu, M. Generalized cross entropy loss for training deep neural networks with noisy labels. *Advances in neural information processing systems* **31** (2018).
- 56 Ruby, U. & Yendapalli, V. Binary cross entropy with deep learning technique for image classification. *Int. J. Adv. Trends Comput. Sci. Eng* **9** (2020).
- 57 Zaheer, R. & Shaziya, H. in *2019 Third International Conference on Inventive Systems and Control (ICISC)*. 536-539.
- 58 Roca, C. P. *et al.* A cross entropy test allows quantitative statistical comparison of t-SNE and UMAP representations. *Cell Reports Methods* **3** (2023).
- 59 Muthuraj, R., Gopal, D., Ahmed, I. & Chandrasekaran, J. Insightful t-SNE guided exploration spotlighting Palbociclib and Ribociclib analogues as novel WEE1 kinase inhibitory candidates. *Journal of Biomolecular Structure and Dynamics*, 1-13, doi:10.1080/07391102.2024.2305316.
- 60 Silva, R. & Melo-Pinto, P. t-SNE: A study on reducing the dimensionality of hyperspectral data for the regression problem of estimating oenological parameters. *Artificial Intelligence in Agriculture* **7**, 58-68, doi:<https://doi.org/10.1016/j.aiia.2023.02.003> (2023).
- 61 Li, S., Li, T., Sun, C., Yan, R. & Chen, X. Multilayer Grad-CAM: An effective tool towards explainable deep neural networks for intelligent fault diagnosis. *Journal of Manufacturing Systems* **69**, 20-30, doi:<https://doi.org/10.1016/j.jmsy.2023.05.027> (2023).
- 62 Zhang, H. & Ogasawara, K. Grad-CAM-Based Explainable Artificial Intelligence Related to Medical Text Processing. *Bioengineering* **10** (2023).

- 63 van Zyl, C., Ye, X. & Naidoo, R. Harnessing eXplainable artificial intelligence for feature selection in time series energy forecasting: A comparative analysis of Grad-CAM and SHAP. *Applied Energy* **353**, 122079, doi:<https://doi.org/10.1016/j.apenergy.2023.122079> (2024).
- 64 Chen, Y. Z., Jiang, H. C., Jiang, S. W., Liu, X. Z. & Zhang, W. L. Thin film thermocouples for surface temperature measurement of turbine blade. *Advanced Materials Research* **873**, 420-425 (2014).
- 65 Ruan, Y., Li, J., Xiao, Q., Wu, Y. & Shi, M. High-Temperature Failure Evolution Analysis of K-Type Film Thermocouples. *Micromachines* **14** (2023).
- 66 Chu, L., Arzberger, M., Böhm, G. & Abstreiter, G. Influence of growth conditions on the photoluminescence of self-assembled InAs/GaAs quantum dots. *Journal of Applied Physics* **85**, 2355-2362, doi:10.1063/1.369549 (1999).
- 67 Suekane, O., Hasegawa, S., Okui, T., Takata, M. & Nakashima, H. Growth Temperature Dependence of InAs Islands Grown on GaAs (001) Substrates. *Japanese Journal of Applied Physics* **41**, 1022, doi:10.1143/JJAP.41.1022 (2002).
- 68 Cheng, Y., Wang, D., Zhou, P. & Zhang, T. in *arxiv* <https://arxiv.org/abs/1710.09282> (2017).
- 69 Sutton, R. S. Learning to predict by the methods of temporal differences. *Machine Learning* **3**, 9-44, doi:10.1007/bf00115009 (1988).
- 70 Vamathevan, J. *et al.* Applications of machine learning in drug discovery and development. *Nat Rev Drug Discov* **18**, 463-477, doi:10.1038/s41573-019-0024-5 (2019).
- 71 Joyce, T. B. & Bullough, T. J. Beam equivalent pressure measurements in chemical beam epitaxy. *Journal of Crystal Growth* **127**, 265-269, doi:10.1016/0022-0248(93)90619-8 (1993).

Acknowledgements

This work was supported by Beijing Natural Science Foundation (Grant No. L248103, C. Z.), the National Key R&D Program of China (Grant No. 2023YFB2805900, S. M. C.; 2021YFB2206500, C. Z.), National Natural Science Foundation of China (Grant No. 62274159, C. Z.; 62204072, J. N. D), and CAS Project for Young Scientists in Basic Research (Grant No. YSBR-056, C. Z.).

Author Contributions Statement

C. Z. conceived the idea, designed the investigations and the growth experiments. C. S., and W. K. Z. performed the molecular beam epitaxial growth. C. S., and K. Y. X. did the sample characterization. C. S. and C. Z. wrote the manuscript. C. Z. led the molecular beam epitaxy program. B. X. and Z. G. W. supervised the team. All authors have read, contributed to, and approved the final version of the manuscript.

Competing Interests Statement

The authors declare no competing interests.

Supplementary Information

Details on the platform environment and program interface, the functional interface switch in the program, the deployment environment and hardware wiring scheme, the surface morphology of GaAs after observation of $(n \times 6)$, the comparison results from different function fits, the surface morphology and crystal quality of GaAs grown at different temperatures, the variation in QD density with thermocouple temperature, the reference sample prepared using conventional

methods, the reference sample prepared using parameter initialization, and the time-resolved photoluminescence results. The video demonstrated enabling material growth through SemiEpi.

TOC

